HHS Public Access

Author manuscript

Histopathology. Author manuscript; available in PMC 2021 March 01.

Published in final edited form as:

Histopathology. 2019 August ; 75(2): 193–201. doi:10.1111/his.13854.

Genomic analysis of recurrences and high-grade forms of polymorphous adenocarcinomas

Ana Paula Martins Sebastiao[1,2,3,*], **Fresia Pareja**[1,*], **Rahul Kumar**[1], **David N. Brown**[1], **Catarina Silveira**[1], **Edaise M. da Silva**[1], **Ju Youn Lee**[1], **Angela Del**[1], **Nora Katabi**[1], **Simion Chiosea**[4], **Britta Weigelt**[1], **Jorge S. Reis-Filho**[1], **Raja R. Seethala**[4]

[1]Department of Pathology, Memorial Sloan Kettering Cancer Center, New York, NY, USA

[2]Post-Graduate Program in Health Sciences, Pontifical Catholic University of Paraná, Curitiba, Paraná, Brazil

[3]Federal University of Paraná, Department of Medical Pathology, Curitiba, Paraná, Brazil

[4]Department of Pathology, University of Pittsburgh Medical Center, Pittsburgh, PA, USA

Abstract

Aim: Polymorphous adenocarcinoma (PAC) usually follows an indolent course, but some cases may display recurrences and high-grade features. The genetic events associated with recurrences and high-grade versions are yet to be defined. Our aim was to determine the genetic underpinning of recurrent PACs of the salivary gland and the repertoire of somatic genetic alterations in cases with high-grade histology.

Methods and Results: Four PACs from three patients, including one case with matching primary and recurrent tumors, one *de novo* high-grade PAC, and a PAC that transformed to a high-grade tumor following multiple recurrences, were subjected to targeted (MSK-IMPACT) or whole-exome sequencing (WES). Both matching primary and recurrent tumor as well as the *de novo* high-grade PAC harbored clonal *PRKD1* E710D hotspot mutations, whereas the PAC that underwent high-grade transformation upon recurrence, which was wild-type for *PRKD1*, harbored a *PRKD2* rearrangement. The PACs analyzed here also harbored mutations targeting cancer genes such as *PIK3CA, SETD2, ARID1A* and *NOTCH2*. A clonal decomposition analysis of the matching primary and recurrent PACs revealed that a minor subclone from the primary tumor became dominant in the recurrent tumor following a clonal selection evolutionary pattern.

Correspondence to: **Raja R. Seethala,** MD PhD, Department of Pathology, UPMC Presbyterian, 200 Lothrop Street, Pittsburgh, PA 15213, USA. Phone: +1 412 628-9550. seethalarr@upmc.edu; **Jorge S. Reis-Filho**, MD PhD FRCPath, Department of Pathology, Memorial Sloan Kettering Cancer Center, 1275 York Avenue, New York, NY 10065, USA. Phone: +1 212 639 8054. reisfilj@mskcc.org.

*These authors contributed equally to this work

AUTHORS' CONTRIBUTIONS

B.W, J.S.R.-F and R.R.S conceived the study. R.R.S provided tissue samples and clinical data. N.K. S.C. and R.R.S. performed the pathology review. A.P.M.S., F.P., C.S., E.M.d.S. and B.W. performed experiments. R.K., D.B. and J.Y.L. and performed bioinformatics analyses. A.P.M.S., F.P., J.S.R.-F. and R.R.S. wrote the first manuscript, which was reviewed by all co-authors.

Conflict of interest: JSR-F report personal/consultancy fees from VolitionRx, Page.AI, Goldman Sachs, Grails, Ventana Medical Systems, Invicro and Genentech, outside the scope of the submitted work. All other authors declare no conflicts of interest.

Conclusions: Our findings demonstrate that recurrent and high-grade PACs are underpinned by *PRKD1* E710D hotspot mutations or *PRKD2* rearrangements, and that recurrences of PACs may stem from the selection of preexisting subclones in the primary tumor.

Keywords

Polymorphous adenocarcinoma; PRKD1; PRKD2; PRKD3; next generation sequencing; whole-exome sequencing

INTRODUCTION

Polymorphous adenocarcinoma (PAC), previously known as polymorphous low-grade adenocarcinoma, was originally described as an infiltrative tumor with a variety of architectural patterns and tumor cells usually showing bland nuclei and scanty to moderate cytoplasm [1]. Although the majority of PACs follow an indolent course, some tumors may display an aggressive behavior, high-grade transformation [2-6], local recurrences and rarely distant metastases [7]. In addition, even high-grade variants of this lesion originally described as an 'intrinsically' low-grade tumor have been described [8].

We have previously shown that PACs are underpinned by pathognomonic *PRKD1* E710D hotspot mutations [9]. Rearrangements involving genes pertaining to the *PRKD* gene family, including *PRKD1, PRKD2* and *PRKD3*, have been described in cribriform adenocarcinoma of the minor salivary glands, a neoplastic entity closely related to PACs [10], and potentially in a subset of PACs lacking hotspot mutations affecting *PRKD1* [10, 11]. Here, we sought to determine the repertoire of somatic genetic alterations of recurrent and/or high-grade PACs of the salivary glands.

MATERIALS AND METHODS

Cases

Slides and formalin-fixed paraffin-embedded (FFPE) tissue blocks were retrieved from the archives of the Department of Pathology of University of Pittsburgh Medical Center Presbyterian (UPMC; Pittsburgh, PA, USA) after approval by the institutional review board (IRB). Four PACs, pertaining to three patients were analyzed, including one matched primary tumor and its recurrence (RS1-T1, RS1-T2), one *de novo* high-grade tumor (RS2T) and one PAC that transformed to high-grade after multiple recurrences (RS3T), for which clinicopathologic features were previously reported prior to transformation [12]. Matched normal tissue was available for the latter two cases. Samples were anonymized prior to analysis. All cases were reviewed by three pathologists specialized in head and neck pathology (RS, SC and NK), and were classified as PAC according to the criteria put forward by the World Health Organization (WHO)[1]. In brief, all tumors displayed architectural diversity and areas of cytonuclear uniformity with ovoid vesicular nuclei. All cases showed prominent S100 reactivity and variable (non-patterned) to negative p63 expression. High-grade was defined by the presence of at least two of the following features: i) Areas that lost cytonuclear uniformity with anisomorphism and at least a 4:1 nuclear size

variability, with or without prominent nucleoli, ii) necrosis, and iii) mitotic rates greater than 5 per 10 high power fields (HPF).

Microdissection and DNA extraction

Tumor tissue and normal tissue samples, when available, were microdissected from five consecutive 8 μm-thick formalin-fixed paraffin-embedded histological sections under a stereomicroscope (Olympus SZ61) to ensure a tumor cell content >80%, as previously described [13]. DNA was extracted using the DNAeasy Blood and Tissue Kit (Qiagen) according to manufacturers' instructions [14].

Massively parallel sequencing and bioinformatics analysis

DNA from tumor and matching normal tissue from RST2 and RST3 was subjected to whole exome sequencing (WES) as previously described [13, 14]. For RS1-T1 and RS1-T2, DNA was not of sufficient yield and/or quality to perform WES; hence, these samples were subjected to targeted massively parallel sequencing using the Memorial Sloan Kettering Mutation Profiling of Actionable Cancer Targets (MSK-IMPACT) assay, which targets all exons and selected introns of 468 cancer genes as previously described [14-16]. Analysis of sequencing data was performed as previously described [13, 14, 17]. In brief, reads were aligned to the reference human genome GRCh37 using the Burrows-Wheeler Aligner (BWA, v0.7.15)[18]. Local realignment, duplicate removal and base quality recalibration were performed using the Genome Analysis Toolkit (GATK, v3.1.1)[19]. Somatic single nucleotide variants (SNVs) were detected by MuTect (v1.0)[20], small insertions and deletions (indels) by Strelka (v2.0.15)[21], VarScan 2 (v2.3.7)[22], Lancet (v1.0.0)[23] and Scalpel (v0.5.3)[24]. Copy number alterations (CNAs) and loss of heterozygosity (LOH) were defined using FACETS [25], as previously described [13, 14, 17]. The cancer cell fraction (CCF) of each mutation was inferred using ABSOLUTE (v1.0.6)[26], and mutation was classified as clonal if its probability of being clonal was >50% [27] or if the lower bound of the 95% confidence interval of its CCF was >90% [28, 29], as described [13, 14, 17]. A combination of mutation function predictors [30] was employed to define the potential functional impact of each missense SNV, as previously described [13]. Mutation hotspots were assigned according to Chang *et al.* [31].

Fluorescence *in situ* hybridization (FISH)

FISH analysis for *PRKD1, PRKD2* and *PRKD3* was performed on 4-μm-thick FFPE sections using dual-color break-apart probes following validated protocols at the MSKCC's Molecular Cytogenetics Core as previously described [32]. The probe mix consisted of bacterial artificial chromosome (BAC) clones mapping to 5′ *PRKD1* (RP11-269C4, RP11-777L23; red) and 3′ *PRKD1* (RP11-684G15, RP11-942P15; green), BAC clones mapping to 5′ *PRKD2* (RP11-846M4, RP11-611I8; red) and 3′ *PRKD2* (RP11-194H9, RP11-210G11; green), and BAC clones mapping to 5′ *PRKD3* (RP11-695L15, RP11-278G12; red) and 3' *PRKD3* (RP11-1130K21, RP11-142K18; green). A minimum of 50 interphase nuclei were analyzed for *PRKD1, PRKD2* or *PRKD3* rearrangements. Samples were considered positive for rearrangement if separation of 5' (red) and 3' (green) signals (>2 signal width apart) was identified in >15% tumor cells.

Clonal frequencies and phylogenetic tree construction

To estimate the clonal architecture and composition of the primary tumor (RS1-T1) and recurrent tumor (RS1-T2) of case RS1, mutant allelic fractions from all somatic mutations were adjusted for tumor cell content, ploidy, local copy number and sequencing errors using PyClone [33] as previously described [13]. To convert the mutant allelic fraction measurements to estimates of clonal frequencies for both primary and recurrent tumors, we applied the Dirichlet process clustering model implemented in PyClone [33], that simultaneously estimates the genotype and clonal frequency given a list of somatic mutations and their local copy number. Purity and ploidy estimates, and modal copy number from ABSOLUTE [26] were employed as the input data for PyClone analysis [33]. Clustering was performed using "mpear" as implemented in PyClone [33]. Maximum parsimony trees were generated as previously described [13]. In brief, binary presence/absence matrices were built from the somatic genetic alterations including SNVs and indels within the clonally-related primary and recurrent PACs, and the trees were constructed as described by Murugaesu et al [34].

RESULTS

Cases

This study included tumors from three patients. The first case corresponds to a primary mixed patterned PAC (RS1-T1) of the right upper lip in an 82-year-old male patient, which recurred 28 months after the initial surgical treatment (RS1-T2). The primary and recurrent lesions displayed similar histologic features, showing various architectural patterns including tubulofascicular, glomerulopapillary and solid areas. Although the tumor cells were ovoid and vesicular, the solid areas displayed uniform nuclear enlargement, high mitotic rates (12 per 10 HPFs) and necrosis (Figures 1A and 1B). The remaining two cases analyzed here consisted of one *de novo* high-grade PAC and one PAC that transformed on recurrence. The *de novo* high-grade PAC (RS2T) originated in the palate of a 58-year-old male patient, and displayed glomerulopapillary-to-solid growth with considerable nuclear size variation and an elevated mitotic rate (8 per 10 HPFs; Figure 1C). The recurrent transformed case (RS3T) corresponded to the fourth locoregional recurrence in the face of a 73-year-old female who originally presented with a palatal tumor 336 months prior to the current case. The recurrent tumor showed tubular, trabecular/canalicular and solid growth with focal necrosis and a mildly elevated mitotic rate (6 per 10 HPFs; Figure 1D).

Genomic analysis of recurrent polymorphous adenocarcinomas of the salivary glands

We subjected the matching primary (RS1-T1) and recurrent (RS1-T2) PACs to MSK-IMPACT sequencing, and the *de novo* high-grade PAC (RS2T) and the recurrent transformed PAC (RS3T) to WES (Supplementary Table S1). Both primary (RS1-T1) and recurrent (RS1-T2) PACs of case RS1, as well as the *de novo* high-grade PAC RS2T, harbored clonal *PRKD1* E710D hotspot mutations, whereas the recurrent PAC RS3T was wild-type for *PRKD1* (Figure 2A and Supplementary Figure 1). The presence/ absence of *PRKD1* E710D hotspot mutations were validated by Sanger sequencing analysis (Figure 2B). To determine whether RS3T, which was found to be wild-type for *PRKD1,* would harbor a *PRKD1*, *PRKD2* or *PRKD3* rearrangement, FISH was performed. This analysis revealed that whilst no *PRKD1* and *PRKD3* rearrangements were identified, RS3T harbored

a rearrangement of *PRKD2* (Figure 2C), consistent with the observation that a subset of PACs lacking the *PRKD1* hotspot mutations harbor rearrangements involving *PRKD1*, *PRKD2* or *PRKD3* [10].

A paucity of somatic genetic alterations was detected in the PACs analyzed. It should be noted, however, that the PACs with *PRKD1* E710D hotspot mutations were also found to harbor mutations targeting cancer genes, including a *PIK3CA* D350G hotspot missense mutation, which has been previously described in salivary ductal carcinoma (c.1049A>G) in association with *ERBB2* amplification [35], an *EIF1AX* R13H hotspot missense mutation, a *SETD2* L2012Wfs*7 frameshift mutation, a Q288Pfs*71 frameshift deletion targeting the chromatin remodeling gene *ARID1A*, which has been previously reported in tumors of the salivary gland [16], and an *ERBB2* V839M likely-pathogenic missense mutation targeting its tyrosine kinase domain (Figure 2A and Supplementary Table S2). In addition to the *PRKD2* rearrangement, the recurrent PAC RS3T also harbored a clonal *NOTCH2* Q2409* truncating mutation and a *MEF2B* P315Qfs* frameshift mutation (Figure 2A and Supplementary Table S2). Mutations affecting genes of the Notch signaling pathway have been described in salivary gland cancers, particularly in adenoid cystic carcinoma [36-38]. Consistent with the previously described paucity of gene copy number alterations in PACs [9, 39], the gene copy number analysis performed here did not reveal complex patterns of copy numbers alterations or any recurrent copy number alteration, despite the fact that all PACs analyzed here were of high-grade histologically (Figure 3).

Recurrence of polymorphous adenocarcinomas of the salivary gland involves clonal selection

A clonal decomposition analysis of the somatic mutations of the matching primary (RS1T1) and recurrent (RS1T2) PACs revealed intra-tumor genetic heterogeneity in both lesions. Truncal clonal mutations included *PRKD1* E710D and *EIF1AX* R13H, suggesting that these mutations were early events in the genesis of these tumors. A minor subclone in the primary tumor (RS1T1), which harbored mutations in *PIK3CA* (D350G) and *SETD2* (L2012Wfs*7), became dominant in the recurrent tumor (RS1T2; Figure 4). The recurrent PAC (RS1T2) acquired additional mutations in *ZFHX3* (G3527dup) and *ERBB2* (V839M). Taken together, these findings suggest that in this recurrent PAC, recurrence stemmed from a minor subclone from the primary tumor.

DISCUSSION

Akin to other forms of salivary gland tumors, which have been shown to be driven by highly recurrent if not pathognomonic somatic genetic alterations [40], PACs have been shown to be underpinned by a *PRKD1* hotspot mutation (E710D), which is present in >70% of cases [9]. In the remaining cases, *PRKD2* or *PRKD3* hotspot mutations have not been detected [11]; rather *PRKD1, PRKD2* or *PRKD3* rearrangements with a multitude of 5’ partners have been identified [10]. Given the diversity of histologic patterns observed in PACs, these genetic alterations have proved helpful in diagnosing these lesions. Here, we have employed these molecular characteristics of PACs to define the repertoire of genetic alterations of PACs that have recurred and/or displayed high-grade histologic features.

Our analyses revealed that consistent with primary PACs, recurrent PACs also displayed the canonical alterations affecting PRKD genes, including *PRKD1* hotspot E710D mutations or a *PRKD2* rearrangement. The maintenance of the highly recurrent/pathognomonic genetic alteration that characterizes these tumors in the recurrences and after the acquisition of high-grade histologic features is consistent with the observations made in other tumor types driven by pathognomonic genetic alterations [41-44] and is consistent with the notion that these alterations constitute drivers of the disease. For instance, in the progression of adenoid cystic carcinomas to high-grade tumors, the *MYB-NFIB* fusion genes is maintained [41]; likewise, in the progression of granulosa cell tumors, the *FOXL2* C134W mutation is conserved [42-44]. Consistent with the notion that in the progression of tumors driven by pathognomonic mutations, additional genetic alterations are acquired or subclonal genetic alterations present in minor subclones of the primary tumor are selected [41-44], we observed that the recurrent tumor RS1T2 acquired additional subclonal *ERBB2* (V839M) and *ZFHX3* (G3527dup) mutations. Moreover, our analyses revealed that a minor sub-clone of the primary tumor (RS1T1), which harbored the *PIK3CA* D350G hotspot mutation, became dominant in the recurrent tumor (RS1T2; Figure 4), suggesting that recurrence of PACs may be driven by selection of pre-existing subclones.

Our study has important limitations. First, owing to the rarity of high grade PACs, the sample size is small. Hence, the biological and clinical significance of the somatic genetic alterations in addition to those affecting *PRKD1/2/3* remains to be defined. Second, we could not establish the fusion partner of *PRKD2* in the rearrangement identified in the recurrent PAC wild-type for *PRKD1*, due to insufficient material to conduct RNA sequencing analysis. Third, we could not perform a clonal decomposition analysis for recurrent PACs RS3T given the lack of a matching primary tumor sample. Despite the limitations of our study, our findings support the notion that, in a way akin to primary tumors, recurrent PACs are underpinned by *PRKD1* E710D hotspot mutations or rearrangements involving members of the PRKD family. Moreover, our analysis revealed that recurrences may be driven by clonal selection of preexisting subclones of the primary tumor.

Supplementary Material

Refer to Web version on PubMed Central for supplementary material.

ACKNOWLEDGEMENTS

We thank the Molecular Cytogenetics Core from MSKCC for their technical assistance. Research reported in this publication was partly funded by a Cancer Center Support Grant of the National Institutes of Health/National Cancer Institute (grant No P30CA008748). The content is solely the responsibility of the authors and does not necessarily represent the official views of the National Institutes of Health. JSR-F is partly funded by the Breast Cancer Research Foundation, BW by Cycle for Survival.

REFERENCES

1. El-Naggar AK C J, Grandis JR, Takata T, Slootweg PJ. Who classification of head and neck tumours. Lyon, 2017.
2. Mills SE, Garland TA, Allen MS. Low-grade papillary adenocarcinoma of palatal salivary gland origin. Am J Surg Pathol 1984;8;367–374. [PubMed: 6731663]

3. Lloreta J, Serrano S, Corominas JM, Ferrés-Padró E. Polymorphous low-grade adenocarcinoma arising in the nasal cavities with an associated undifferentiated carcinoma. Ultrastruct Pathol 1995;19;365–370. [PubMed: 7483012]
4. Pelkey TJ, Mills SE. Histologic transformation of polymorphous low-grade adenocarcinoma of salivary gland. Am J Clin Pathol 1999;111;785–791. [PubMed: 10361514]
5. Simpson RH, Pereira EM, Ribeiro AC, Abdulkadir A, Reis-Filho JS. Polymorphous low-grade adenocarcinoma of the salivary glands with transformation to high-grade carcinoma. Histopathology 2002;41;250–259. [PubMed: 12207787]
6. Xu B, Aneja A, Ghossein R, Katabi N. Predictors of outcome in the phenotypic spectrum of polymorphous low-grade adenocarcinoma (plga) and cribriform adenocarcinoma of salivary gland (casg): A retrospective study of 69 patients. Am J Surg Pathol 2016;40;1526–1537. [PubMed: 27454943]
7. Castle JT, Thompson LD, Frommelt RA, Wenig BM, Kessler HP. Polymorphous low grade adenocarcinoma: A clinicopathologic study of 164 cases. Cancer 1999;86;207–219. [PubMed: 10421256]
8. Seethala RR. An update on grading of salivary gland carcinomas. Head Neck Pathol 2009;3;69–77. [PubMed: 20596994]
9. Weinreb I, Piscuoglio S, Martelotto LG et al. Hotspot activating prkd1 somatic mutations in polymorphous low-grade adenocarcinomas of the salivary glands. Nat Genet 2014;46;1166–1169. [PubMed: 25240283]
10. Weinreb I, Zhang L, Tirunagari LM et al. Novel prkd gene rearrangements and variant fusions in cribriform adenocarcinoma of salivary gland origin. Genes Chromosomes Cancer 2014;53;845–856. [PubMed: 24942367]
11. Piscuoglio S, Fusco N, Ng CK et al. Lack of prkd2 and prkd3 kinase domain somatic mutations in prkd1 wild-type classic polymorphous low-grade adenocarcinomas of the salivary gland. Histopathology 2016;68;1055–1062. [PubMed: 26426580]
12. Seethala RR, Johnson JT, Barnes EL, Myers EN. Polymorphous low-grade adenocarcinoma: The university of pittsburgh experience. Arch Otolaryngol Head Neck Surg 2010;136;385–392. [PubMed: 20403856]
13. Geyer FC, Li A, Papanastasiou AD et al. Recurrent hotspot mutations in hras q61 and pi3k-akt pathway genes as drivers of breast adenomyoepitheliomas. Nat Commun 2018;9;1816. [PubMed: 29739933]
14. Pareja F, Brandes AH, Basili T et al. Loss-of-function mutations in atp6ap1 and atp6ap2 in granular cell tumors. Nat Commun 2018;9;3533. [PubMed: 30166553]
15. Schultheis AM, Ng CK, De Filippo MR et al. Massively parallel sequencing-based clonality analysis of synchronous endometrioid endometrial and ovarian carcinomas. J Natl Cancer Inst 2016;108;djv427. [PubMed: 26832770]
16. Zehir A, Benayed R, Shah RH et al. Mutational landscape of metastatic cancer revealed from prospective clinical sequencing of 10,000 patients. Nat Med 2017;23;703–713. [PubMed: 28481359]
17. Ng CKY, Bidard FC, Piscuoglio S et al. Genetic heterogeneity in therapy-naïve synchronous primary breast cancers and their metastases. Clin Cancer Res 2017;23;4402–4415. [PubMed: 28351929]
18. Li H, Durbin R. Fast and accurate long-read alignment with burrows-wheeler transform. Bioinformatics 2010;26;589–595. [PubMed: 20080505]
19. McKenna A, Hanna M, Banks E et al. The genome analysis toolkit: A mapreduce framework for analyzing next-generation DNA sequencing data. Genome Res 2010;20;1297–1303. [PubMed: 20644199]
20. Cibulskis K, Lawrence MS, Carter SL et al. Sensitive detection of somatic point mutations in impure and heterogeneous cancer samples. Nat Biotechnol 2013;31;213–219. [PubMed: 23396013]
21. Saunders CT, Wong WS, Swamy S, Becq J, Murray LJ, Cheetham RK. Strelka: Accurate somatic small-variant calling from sequenced tumor-normal sample pairs. Bioinformatics 2012;28;1811–1817. [PubMed: 22581179]

22. Koboldt DC, Zhang Q, Larson DE et al. Varscan 2: Somatic mutation and copy number alteration discovery in cancer by exome sequencing. Genome Res 2012;22;568–576. [PubMed: 22300766]
23. Narzisi G, Corvelo A, Arora K et al. Genome-wide somatic variant calling using localized colored de bruijn graphs. Communications Biology 2018;1;20. [PubMed: 30271907]
24. Narzisi G, O'Rawe JA, Iossifov I et al. Accurate de novo and transmitted indel detection in exome-capture data using microassembly. Nat Methods 2014;11;1033–1036. [PubMed: 25128977]
25. Shen R, Seshan VE. Facets: Allele-specific copy number and clonal heterogeneity analysis tool for high-throughput DNA sequencing. Nucleic Acids Res 2016;44;e131. [PubMed: 27270079]
26. Carter SL, Cibulskis K, Helman E et al. Absolute quantification of somatic DNA alterations in human cancer. Nat Biotechnol 2012;30;413–421. [PubMed: 22544022]
27. Landau DA, Carter SL, Stojanov P et al. Evolution and impact of subclonal mutations in chronic lymphocytic leukemia. Cell 2013;152;714–726. [PubMed: 23415222]
28. Ngan E, Stoletov K, Smith HW et al. Lpp is a src substrate required for invadopodia formation and efficient breast cancer lung metastasis. Nat Commun 2017;8;15059. [PubMed: 28436416]
29. Martelotto LG, Baslan T, Kendall J et al. Whole-genome single-cell copy number profiling from formalin-fixed paraffin-embedded samples. Nat Med 2017;23;376–385. [PubMed: 28165479]
30. Martelotto LG, Ng CK, De Filippo MR et al. Benchmarking mutation effect prediction algorithms using functionally validated cancer-related missense mutations. Genome Biol 2014;15;484. [PubMed: 25348012]
31. Chang MT, Bhattarai TS, Schram AM et al. Accelerating discovery of functional mutant alleles in cancer. Cancer Discov 2018;8;174–183. [PubMed: 29247016]
32. Piscuoglio S, Burke KA, Ng CK et al. Uterine adenosarcomas are mesenchymal neoplasms. J Pathol 2016;238;381–388. [PubMed: 26592504]
33. Roth A, Khattra J, Yap D et al. Pyclone: Statistical inference of clonal population structure in cancer. Nat Methods 2014;11;396–398. [PubMed: 24633410]
34. Murugaesu N, Wilson GA, Birkbak NJ et al. Tracking the genomic evolution of esophageal adenocarcinoma through neoadjuvant chemotherapy. Cancer Discov 2015;5;821–831. [PubMed: 26003801]
35. Dalin MG, Desrichard A, Katabi N et al. Comprehensive molecular characterization of salivary duct carcinoma reveals actionable targets and similarity to apocrine breast cancer. Clin Cancer Res 2016;22;4623–4633. [PubMed: 27103403]
36. Dang H, Lin AL, Zhang B, Zhang HM, Katz MS, Yeh CK. Role for notch signaling in salivary acinar cell growth and differentiation. Dev Dyn 2009;238;724–731. [PubMed: 19235730]
37. Stephens PJ, Davies HR, Mitani Y et al. Whole exome sequencing of adenoid cystic carcinoma. J Clin Invest 2013;123;2965–2968. [PubMed: 23778141]
38. Rettig EM, Talbot CC, Sausen M et al. Whole-genome sequencing of salivary gland adenoid cystic carcinoma. Cancer Prev Res (Phila) 2016;9;265–274. [PubMed: 26862087]
39. Persson F, Fehr A, Sundelin K, Schulte B, Löning T, Stenman G. Studies of genomic imbalances and the myb-nfib gene fusion in polymorphous low-grade adenocarcinoma of the head and neck. Int J Oncol 2012;40;80–84. [PubMed: 21901247]
40. Skálová A, Stenman G, Simpson RHW et al. The role of molecular testing in the differential diagnosis of salivary gland carcinomas. Am J Surg Pathol 2018;42;e11–e27. [PubMed: 29076877]
41. Fusco N, Geyer FC, De Filippo MR et al. Genetic events in the progression of adenoid cystic carcinoma of the breast to high-grade triple-negative breast cancer. Mod Pathol 2016;29;1292–1305. [PubMed: 27491809]
42. Yanagida S, Anglesio MS, Nazeran TM et al. Clinical and genetic analysis of recurrent adult-type granulosa cell tumor of the ovary: Persistent preservation of heterozygous c.402c>g foxl2 mutation. PLoS One 2017;12;e0178989. [PubMed: 28594898]
43. Hillman RT, Celestino J, Terranova C et al. Kmt2d/mll2 inactivation is associated with recurrence in adult-type granulosa cell tumors of the ovary. Nat Commun 2018;9;2496. [PubMed: 29950560]
44. Alexiadis M, Rowley SM, Chu S et al. Mutational landscape of ovarian adult granulosa cell tumors from whole exome and targeted tert promoter sequencing. Mol Cancer Res 2018.

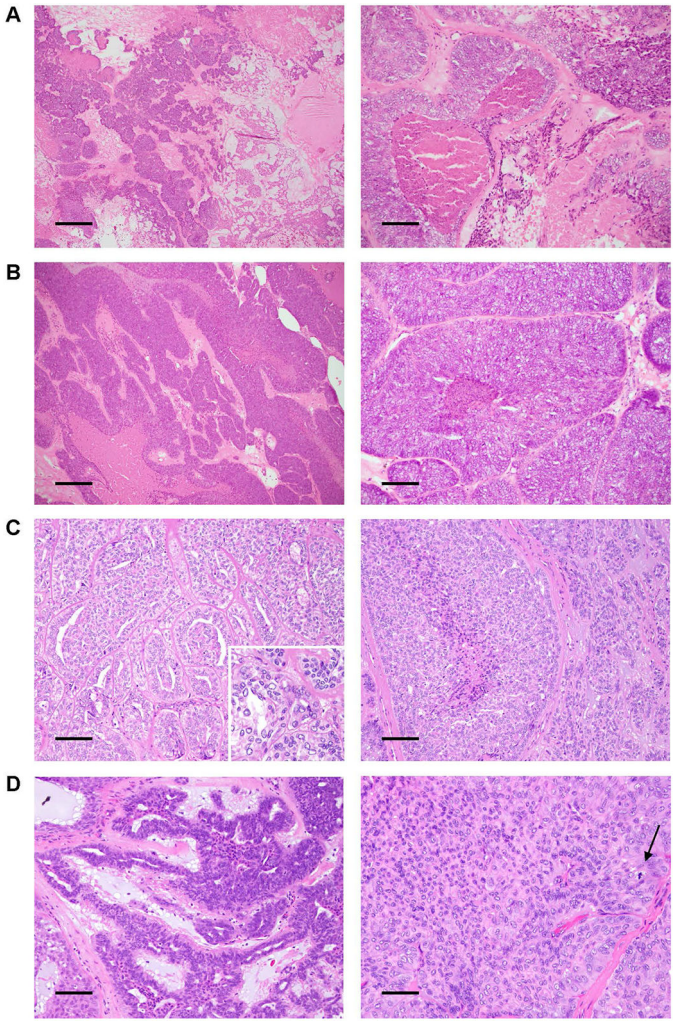

Figure 1. Histologic features of recurrent polymorphous adenocarcinomas (PACs) of the salivary gland.

(A-B) Representative hematoxylin and eosin (H&E) photomicrographs of matched primary (RS1-T1) and recurrent (RS1-T2) PACs with high-grade histologic features. **(A)** Low-power magnification of RS1-T1 (left), a heterogeneous lesion with intermingled hypocellular and hypercellular areas displaying high-grade features (scale bar, 500 μm). Intermediate-power magnification of RS1-T1 (right) displaying a solid architecture, conspicuous nucleoli, frequent mitoses and necrosis (scale bar, 100 μm) **(B)** Low-power magnification of the recurrent high-grade PAC (RS1-T2; left) displaying solid architecture with extensive necrosis (scale bar, 200 μm). Intermediate-power magnification of RS1-T2 (right) showing frequent mitoses and focal necrosis (scale bar, 100 μm). **(C)** Representative H&E photomicrographs of a *de novo* high-grade PAC (RS2T; left) showing glomerulopapillary growth pattern (scale bar, 200 μm). The inset shows pronounced nuclear size variation. Intermediate-power magnification of RS2T (right) showing focal necrosis (scale bar, 200 μm). **(D)** Representative H&E photomicrographs of RS3T, a PAC that transformed upon recurrence (left), displaying tubular and canalicular architectural patterns with myxoid

stroma (scale bar, 200 μm). High-power magnification of RS3T (right) showing solid growth, nuclear size variation and mitoses (arrow; scale bar, 100 μm).

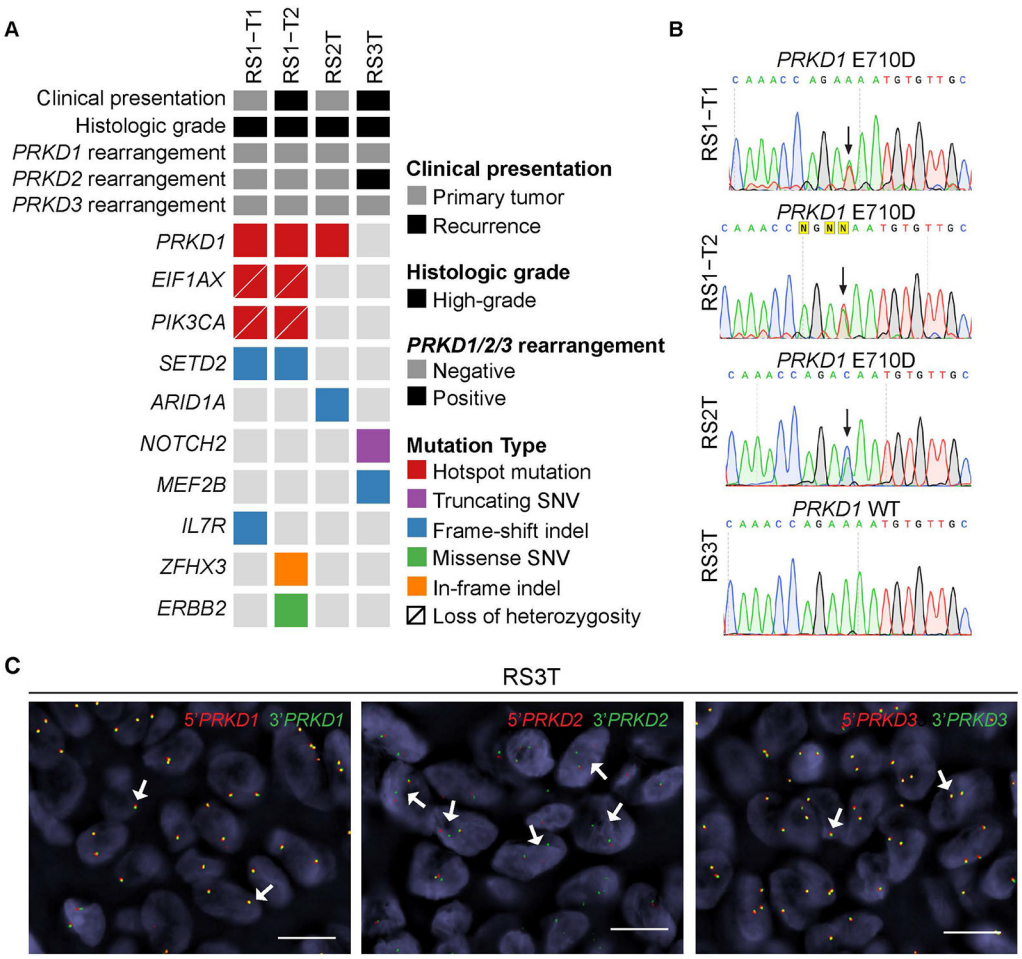

Figure 2. Recurrent polymorphous adenocarcinoma (PAC) of the salivary glands harbor recurrent *PRKD1* E710D hotspot somatic mutations or rearrangements of PRKD genes, and mutations in other cancer genes.

(A) Somatic mutations identified in primary and recurrent PACs by whole-exome (n=2) or MSK-IMPACT sequencing (n=2). Cases are shown in columns and genes in rows. Clinical presentation, histologic grade, and presence of *PRKD2* rearrangement are shown in phenotype bars (top). Mutation types are color-coded according to the legend. **(B)** Representative Sanger sequencing electropherograms of *PRKD1*. **(C)** Representative micrographs of fluorescence *in situ* hybridization (FISH) for *PRKD1*, *PRKD2* and *PRKD3* in recurrent *PRKD1* wild-type PAC (RS3T). Arrows highlight the break-apart red and green signals in one allele, consistent with *PRKD2* rearrangement (middle) or the close or overlapping red and green signals consistent with no *PRKD1* (left) or *PRKD3* (right) rearrangement. Scale bars, 10 μm. SNV, single nucleotide variation.

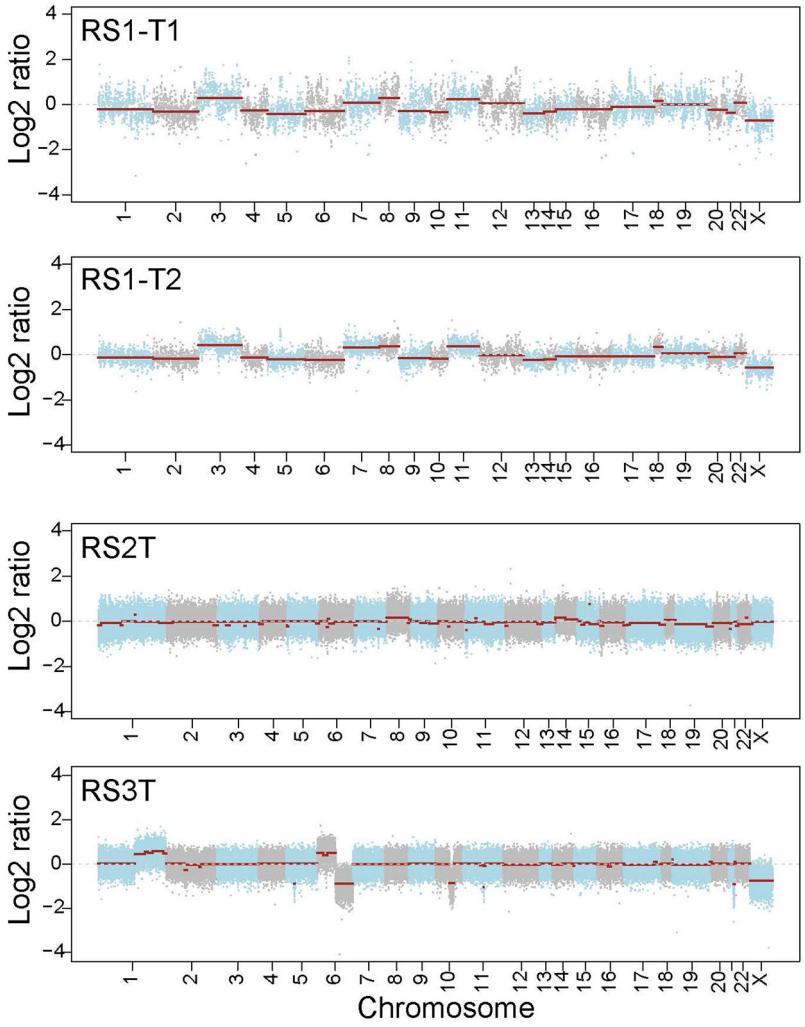

Figure 3. Copy number profiles of polymorphous adenocarcinomas subjected to MSK-IMPACT (n=2) or whole-exome sequencing (n=2).

Copy number plots depicting segmented Log2 ratios (*y*-axis) plotted according to their genomic positions (*x*-axis). Alternating blue and gray demarcate the chromosomes. Note the lack of any high-level gene amplifications or homozygous deletions.

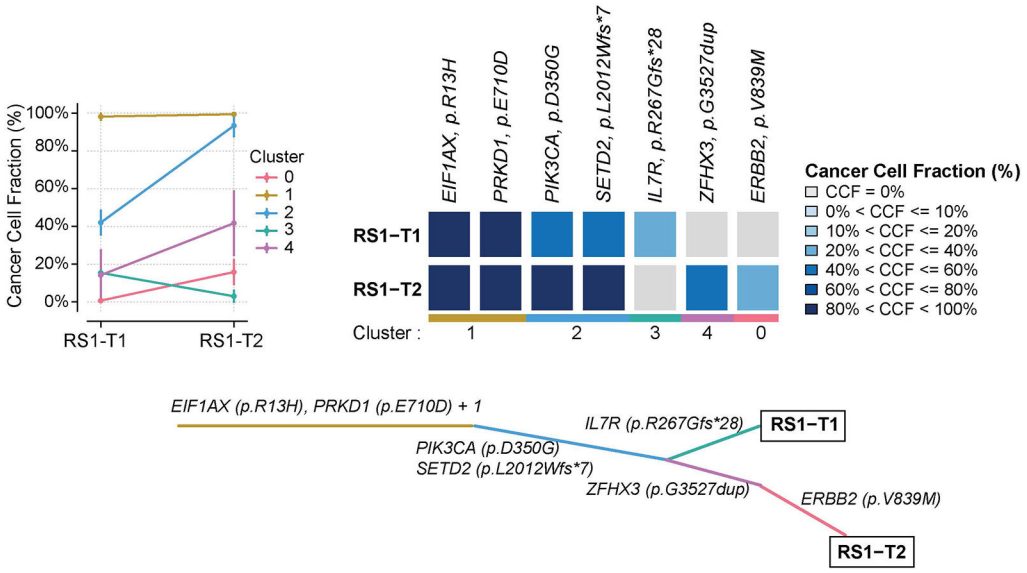

Figure 4. Clonal composition of a matched primary and recurrent polymorphous adenocarcinoma (PAC).

Clonal frequency heatmaps of mutations in a matched primary (RS1-T1) and recurrent (RS1-T2) PAC, grouped by their clonal/subclonal structure (clusters) as inferred by Pyclone[33] (top right). Cancer cell fractions are color-coded according to the legend in the right-hand side. PyClone clusters are shown across the bottom of the clonal frequency heatmap. Parallel coordinates plot generated by PyClone (top left) and cluster-based phylogenetic tree (bottom) of matched primary and recurrent polymorphous adenocarcinomas. Trunk and branches are colored according to cluster as per PyClone. The branch lengths are proportional to the number of genetic alterations. CCF, cancer cell fraction.